Layered superconductors. II. Melting of parallel-flux lattice

Baruch Horovitz
Department of Physics, Ben-Gurion University, Beer-Sheva 84105, Israel
(Received 28 July 1992)

A system of superconducting layers with Josephson coupling J between neighboring layers is studied in the presence of a magnetic field parallel to the layers. A sequence of "ℓ phases" is produced where the induced flux lines are ℓ layers apart. An ℓ phase is solved by an equivalent fermion problem and its melting temperature $T_m(\ell)$ is found. When J is not too small, there is a range $\ell_{\min} < \ell < \ell_{\max}$ for which two-dimensional phases are possible and $\ell_{\min} = 8-10$. These results account for the current-voltage relation of the form $V \sim I^{a(T)}$ as observed in many of the high-T_c superconductors.

I. INTRODUCTION

The anisotropic properties of most of the high-temperature oxide superconductors has led to increased interest in the effects of two-dimensional (2D) fluctuations. In particular, data on thin films of a variety of compounds[1-13] have shown typical behavior of a two-dimensional superconductor. This behavior corresponds to a Kosterlitz-Thouless[14] and Berezinskii-type[15] phase transition where vortices are thermally excited above a critical temperature T_v. The presence of this transition is observed in two ways:[16] (i) Resistivity ρ_v of free vortices at $T > T_v$, which has the form

$$\rho_v \sim \exp\{-2[b(T_c^0 - T)/(T - T_v)]^{1/2}\} , \quad T_c^0 > T > T_v , \tag{1}$$

where b is a constant and T_c^0 is the mean-field transition temperature. (ii) Unbinding of vortices by the current at $T < T_v$, leading to current-(I) voltage (V) relation of the form

$$V \sim I^{a(T)}, \quad T < T_v . \tag{2}$$

The exponent $a(T)$ jumps from 1 to 3 at T_v and increases at lower temperatures; the extrapolation of a $a(T)$ to 1 yields T_c^0.

The relations (1) and (2) were observed in thin films of $Bi_2Sr_2CaCu_2O_x$ (Ref. 1), $Tl_2Ba_2CaCu_2O_8$ (Ref. 2), $YBa_2Cu_3O_x$,[3-6] and $YBa_2Cu_3O_7/PrBa_2Cu_3O_7$ superlattices;[7] in some cases,[8,9] Eq. (1) was observed without the behavior (2). Note that the critical temperature T_v is usually considered as the superconducting transition temperature T_c; strictly speaking, T_c should be the onset of a finite critical current, signaling a three-dimensional (3D) superconductor and is therefore distinct from T_v.

Of additional interest are reports on the observation of Eq. (2) in magnetic fields perpendicular to the layers in $ErBa_2Cu_3O_7$ (Ref. 10) and $Bi_2Sr_2CaCu_2O_x$ (Ref. 11) as well as with magnetic fields parallel to the layers in $Bi_2Sr_2CaCu_2O_x$.[12,13] Of particular interest is the data[11] which show a strong decrease of the exponent $a(T)$ when a perpendicular magnetic field is increased up to 15 G. The other experiments[10,12,13] observe Eq. (2) at much higher fields and at temperatures well below T_c.

The values of T_v and of T_c^0 as deduced from Eq. (2) can determine the thickness of a fluctuating 2D superconducting layer. In the preceding companion paper,[17] referred to as I below, it was shown that [Eq. (35) of I, neglecting the fugacity term]

$$T_v = (\tau/8)\ell_{\text{eff}} , \tag{3}$$

where $\tau = \phi_0^2 d/4\pi^2\lambda_{ab}^2$, ϕ_0 is the flux quantum, λ_{ab} is the magnetic penetration length, and d is the average spacing between CuO_2 layers; ℓ_{eff} is the number of CuO_2 layers which fluctuate as one effective layer. Parametrizing $\lambda_{ab} = \lambda'(1 - T/T_c^0)^{-1/2}$ with λ' known from μSR data,[18] Eq. (3) determines ℓ_{eff} from known data, as shown in Table I. Thus ℓ_{eff} is much less than the number of layers in the samples, though it is larger than 1; i.e., a few CuO_2 layers fluctuate coherently as a single effective layer. The CuO_2 layers form evenly spaced bilayers (i.e., a shorter spacing within the bilayer); if one considers a bilayer as the thinnest layer, Table I should have d larger by factor 2 and ℓ_{eff} smaller by factor 2, the latter value is still larger than 1.

The lower limit of the current, $I_{\min}$, where Eq. (2) is

TABLE I. $V \sim I^{a(T)}$ data analysis. Values of ℓ_{eff} are determined by Eq. (3), $r_{\max}$ from Eq. (4), and r_J from Eq. (5). The forms $\lambda_{ab} = \lambda'(1 - T/T_c^0)^{-1/2}$ and $\xi_0 \approx 15(1 - T/T_c^0)^{-1/2}$ Å were assumed, where λ' is fitted from the T_c vs λ_{ab} of Ref. 18. J is estimated from anisotropy data (Sec. VI of I), and d is the average spacing of CuO_2 layers.

Material	Ref.	T_c^0 (K)	T_v (K)	J (K)	d (Å)	λ' (Å)	ℓ_{eff}	$r_{\max}/\xi_0$	r_J/ξ_0
$Bi_2Sr_2CaCu_2O_x$	1	81.8	78.6	0.1	7.7	1700	8.4	10^4	10^2
$Tl_2Ba_2CaCu_2O_8$	2	100.2	99.0	0.01	7.4	~1100	14.5	10^5	10^3
$YBa_2Cu_3O_7$	4	85.95	83.45	10	5.9	~1100	6.2	10^3	1
$YBa_2Cu_3O_7$	6	90.2	89.1	10	5.9	900	10.8	10^3	1

observed defines a maximal scale $r_{\max}$ at which vortices interact logarithmically and where the 2D type of vortex unbinding is observed. This scale is given by[1]

$$r_{\max}=\phi_0 c L_1/(16\pi^2\lambda_{ab} I_{\min}) , \tag{4}$$

where L_1 is the sample length perpendicular to the current (when the film thickness W is less than λ_{ab}, a factor W/λ_{ab} is needed, though it is usually[1-3] close to 1). On the other hand, when the Josephson coupling J between layers is finite, it sets a potential linear in the vortex separation r. Hence, beyond some scale r_J, the Josephson coupling dominates and Eq. (2) can hold if $r_{\max}<r_J$. The linear potential is the energy of a flux line parallel to the layers, which per unit length is $H_{c1}\phi_0/4\pi$. Using the mean field result[19] $H_{c1}=(\pi Jd/\lambda_{ab}^2\xi_0^2)^{1/2}\ln\lambda_{ab}/\xi_0$ and comparing it to the vortex-vortex interaction $(\tau/2)\ln(r/\xi_0)$ [Eq. (20a) of I], where ξ_0 is the (temperature-dependent) coherence length, yields for T near T_v

$$(r_J/\xi_0)\ln^{-1}(r_J/\xi_0)\approx 0.4(T_v/J)^{1/2} , \tag{5}$$

where $\lambda_{ab}/\xi_0\approx 100$ in the $\ln\lambda_{ab}/\xi_0$ factor of H_{c1} (Ref. 19) was assumed. Note that the Josephson coupling is defined per area ξ_0^2 [Eq. (3) of I] so that for SIS-type junction J should be weakly temperature dependent. Using then the estimates for J (Sec. VI of I) and the observed $I_{\min}$ yields values of $r_{\max}\gg r_J$ as shown in Table I, with $r_{\max}/r_J$ as large as 10^2. This is a remarkable discrepancy—vortices interact logarithmically via Eq. (2) at distances where the Josephson coupling should dominate. In fact, Artemenko and Latyshev[1] noticed this difficulty and argued that some type of thermal fluctuations must reduce J.

Furthermore, data on superlattices such as $(YBa_2Cu_3O_7)_m(PrBa_2Cu_3O_7)_n$, as discussed in I, shows a significant reduction in T_c as n increases, indicating that J is a significant factor in determining T_c; the presence of a 2D phenomena is therefore unexpected.

The objective of the present work is to find situations in which a $J\neq 0$ system can have 2D phases in a strict sense. In the preceding companion paper,[17] the phase transition in anisotropic layered superconductors is studied. It is shown there that the transition temperature T_c is in principle a 3D transition even if J is small. T_c is determined by a competition between fluctuations of two types of topological excitations: $\pm 2\pi$ phase singularities, termed here vortices, and Josephson vortices, i.e., $\pm 2\pi$ phase variations of the relative phase of neighboring layers, termed here fluxons.

Considerable insight on fluctuation phenomena is gained by studying a layered superconductor in a magnetic field parallel to the layers. Fluctuations of flux lines in between layers may weaken the interlayer coupling and lead to a 2D phase. In fact, Efetov[19] has proposed that above some critical field ($\gg H_{c1}$) the flux lattice melts, loosing its 3D correlations and therefore allowing for a 2D phase.

Using a fermion representation, I have shown[20] that this melting temperature $T_m^{(1)}$ is finite even in high fields. In fact, $T_m^{(1)}>T_v^{(1)}$, where $T_v^{(1)}$ is the transition temperature of an isolated layer due to in-layer vortex fluctuations. Thus fluxon melting cannot be separated from vortex fluctuations as done in the derivation of $T_m^{(1)}$; a 2D phase does not exist, and the phase transition is a 3D one, in between $T_v^{(1)}$ and $T_m^{(1)}$. This scenario is similar to that in the absence of a magnetic field.[17] Extending the study[20] to lower fields, where fluxon lines are ℓ layers apart, it is found that their melting temperature $T_m^{(\ell)}$ can satisfy $T_v^{(\ell)}<T_m^{(\ell)}$ for $\ell>8$, where $T_v^{(\ell)}$ is the vortex transition temperature for ℓ coupled layers. In the latter case, a strict 2D phase is possible and the I-V data may be understood if some (unintentional) parallel magnetic field is present in the experiment.

Melting of the parallel fluxon lattice was also studied by Mikheev and Kolomeisky[21] considering the fluxon position variables as fermions and concluding that 2D phases are not possible for weak magnetic fields; this is not inconsistent with the above mentioned intermediate field result.[20] Note also that the asssumption[21] of weakly interacting fermions is correct only if a finite J is maintained; however, eventually the approach[21] uses a small-J expansion, which seems inconsistent with weakly interacting fermions. Furthermore, the use of flux-line positions as fermion variables neglects fluxon-loop fluctuations which contribute to layer decoupling.[17]

In a different approach, Korshunov[22] has used an effective free energy for fluxon coordinates claiming that 2D phases are not possible for any ℓ. This approach also neglects fluxon-loop fluctuations, which is probably correct for high fields. In fact, Korshunov and Larkin[23] have used an asymptotic high-field expansion for the original phase variables, avoiding an assumed fluxon coordinate. They find that, for $d\ll\lambda_{ab}$, $T_m^{(1)}/T_v^{(1)}=\frac{8}{3}$; this confirms the absence of a 2D phase for $\ell=1$.

In the present work, a previous Letter[20] is presented in detail. In Sec. II the free energy of M superconducting layers, excluding in-layer vortices, is transformed into a quantum problem of fermions on M chains. These fermions are a precise mapping of the superconducting phases, and no assumption on the presence of fluxon coordinates is necessary. The critical field H_{c1} is found, and a mean-field solution shows the existence of "ℓ phases," i.e., a sequence of phases with fluxon lines ℓ layers apart. The presence of these phases is expected on general grounds in view of the discreteness of the layers. The precise location of these phases is not essential for the following section. Section III solves the fermion problem in an ℓ phase by first linearizing the fermion spectrum around the Fermi points (as determined by the magnetic field) and then deriving renormalization-group (RG) equations to two loops for the interacting fermions. Analytic arguments and numerical solutions determine bounds on the melting temperatures $T_m^{(\ell)}$. Section IV considers the vortex transition $T_v^{(\ell)}$ in a system of ℓ coupled layers based on I and on comparison with Monte Carlo data;[24] the conditions for $T_m^{(\ell)}<T_v^{(\ell)}$ and the resulting 2D phases are discussed. Section V summarizes the experimental data of Table I in view of the present theory.

II. FERMION REPRESENTATION

Consider the problem of superconducting layers with phases $\varphi_n(\mathbf{r})$ on the nth layer at position $\mathbf{r}=(x_1,x_2)$ on the layer. These phases are coupled by a Josephson coupling J and an external magnetic field H is parallel to the layers. The analysis assumes that the phases $\varphi_n(\mathbf{r})$ are nonsingular; i.e., there are no in-layer vortices; these competing vortex excitations are considered in Sec. IV. The problem thus involved fluctuations of both fluxon loops and fluxon lines; the latter are induced by H.

The magnetization of fluxons in the direction parallel to the magnetic field, say, the x_2 direction, is $M_2=(\phi_0/2\pi)\sum_n \partial\theta_n(\mathbf{r})/\partial x_1$ [from summing Eq. (39) of I], where $\theta_n(\mathbf{r})$ is the gauge-invariant relative phase of layers n and $n-1$ [Eq. (5b) of I] and $\phi_0=hc/2e$ is the flux quantum. The effective free energy is obtained from Eq. (15) of I by setting $s_n(r)=0$ (no vortices) and by adding $-HM_2/4\pi$,

$$\mathcal{F}=\int d^2r\left\{\sum_k \tfrac{1}{2}T\beta(k)[\nabla\theta_k(\mathbf{r})]^2-(J/\xi_0^2)\sum_n \cos\theta_n(\mathbf{r}) -(H\phi_0/8\pi^2)\sum_n \partial\theta_n(\mathbf{r})/\partial x_1\right\}, \tag{6}$$

where $\theta_k(\mathbf{r})$ is the Fourier transform of $\theta_n(\mathbf{r})$ with $|k|<\pi/d$ and

$$\beta(k)=\frac{\tau}{4\pi T}\frac{\lambda_e/d}{1+(4\lambda_e/d)\sin^2\frac{1}{2}kd}\ . \tag{7}$$

The notation is the same as in I; i.e., the length scales are λ, the in-layer penetration length; d_0, a layer thickness; $\lambda_e=\lambda^2/d_0$, the effective penetration length; d, the layer spacing; and ξ_0, the in-layer coherence length; typically, $\lambda_e/d=10^5-10^6$. The energy scale is set by $\tau=\phi_0^2/4\pi^2\lambda_e$; note that the experimentally determined λ_{ab} is $\lambda_{ab}=\lambda(d/d_0)^{1/2}$ [see discussion below Eq. (27) of I].

The problem at hand is to evaluate the partition sum of Eq. (6), i.e., integrate $\exp(-F/T)$ over all configurations of $\theta_n(\mathbf{r})$. Except for the k dependence, this problem is similar to that of the commensurate-incommensurate transition in 2D.[25–28] To solve this problem, I use a method close to that of Schulz,[26] a method which was efficient for solving the critical behavior at the commensurate-incommensurate transition.

The problem is first transformed into a quantum problem of a boson field by rewriting the x_2 coordinate as $x_2=it$, where t is the time variable in the quantum problem. F becomes then a Lagrangian $\mathcal{L}$ for a boson field. Defining $\theta_k(q)$ with q the Fourier transform variable of x_1 (the t dependence is implicit) and its conjugate momenta $\pi_k(q)=\delta\mathcal{L}/\delta[\partial\theta_k(q)/\partial t]$ yields the equivalent Hamiltonian for the first term of (6),

$$\mathcal{H}_0=\tfrac{1}{2}\sum_{k,q}\beta^{-1}(k)\{\pi_k(q)\pi_{-k}(-q)+\beta_0^2q^2\theta_k(q)\theta_{-k}(-q) -[\beta_0^2-\beta^2(k)]q^2\theta_k(q)\theta_{-k}(-q)\}\ . \tag{8}$$

The parameter β_0 is, for now, arbitrary. The form of the two last terms in (6) is not affected by this transformation. Define now boson creation and annihilation operators $c_k^\dagger(q)$ and $c_k(q)$ by

$$\theta_k(q)=i(2\beta_0|q|)^{-1/2}[c_k^\dagger(q)-c_{-k}(-q)]\ ,\qquad \pi_k(q)=-(\beta_0|q|/2)^{1/2}[c_k(q)+c_{-k}^\dagger(-q)]\ . \tag{9}$$

Note that β_0 is used in this definition, rather than the original $\beta(k)$; with a k-dependent $\beta(k)$, the following transformation into fermions is not feasible. In terms of the Fourier transformed operators $c_n^\dagger(q),c_n(q)$, Eq. (8) becomes (up to a constant term)

$$H_0=\sum_{n,n',q}|q|\{V_{n-n'}c_n^\dagger(q)c_{n'}(q) -\tfrac{1}{2}U_{n-n'}[c_n^\dagger(q)c_{n'}^\dagger(-q)+c_n(-q)c_{n'}(q)]\}, \tag{10}$$

where, with M as the number of layers,

$$V_n=M^{-1}\sum_k\frac{\beta_0^2+\beta^2(k)}{2\beta_0\beta(k)}\exp(iknd)\ ,\qquad U_n=M^{-1}\sum_k\frac{-\beta_0^2+\beta^2(k)}{2\beta_0\beta(k)}\exp(iknd)\ . \tag{11}$$

Define now density operators in term of fermion annihilation operators $a_n(q),b_n(q)$,

$$\rho_{1,n}(q)=\sum_p a_n^\dagger(p+q)a_n(p)\ ,\qquad \rho_{2,n}(q)=\sum_p b_n^\dagger(p+q)b_n(p)\ , \tag{12}$$

with the well-known commutation relations[29]

$$[\rho_{i,n}(-q),\rho_{i,n'}(q')]=(-)^{i-1}(qL/2\pi)\delta_{n,n'}\delta_{q,q'}\quad (i=1,2), \tag{13}$$

where L is the length in the x_1 direction. Thus the density operators can be related to the previous boson operators via

$$\rho_{1,n}(q)=(|q|L/2\pi)^{1/2}c_n^\dagger(q),\quad q>0\ ,\qquad \rho_{2,n}(q)=-(|q|L/2\pi)^{1/2}c_n^\dagger(q),\quad q<0\ , \tag{14}$$

and $\rho_{i,n}(-q)=\rho_{i,n}^\dagger(q)$ $(i=1,2)$. Equation (10) then has the form

$$H_0=(2\pi/L)\sum_{n,n'}\left\{\sum_{q>0}V_{n-n'}[\rho_{1,n}(q)\rho_{1,n'}(-q)+\rho_{2,n}(-q)\rho_{2,n'}(q)] +\sum_q U_{n-n'}\rho_{1,n}(q)\rho_{2n'}(-q)\right\}. \tag{15}$$

Returning now to the $\cos\theta_n$ term in Eq. (6), the fermion-boson transformation is required,[30,31]

$$\psi_{i,n}(x_1)=(2\pi\alpha)^{-1/2}\exp[\pm\phi_{i,n}(x_1)]\ , \tag{16}$$

with the upper (lower) sign for $i=1$ $(i=2)$ and

$$\phi_{i,n}(x_1)=(2\pi/L)\sum_q q^{-1}\rho_{i,n}(q)\exp[-\tfrac{1}{2}\alpha|q|-iqx_1] \quad (i=1,2) . \tag{17}$$

The parameter α in (16) is a momentum cutoff, i.e., $\alpha\approx\xi_0$, and the representation (16) is valid in the limit $\alpha\to 0$. The precise definition of α is not significant here since the phase transition, as obtained in Sec. III, is insensitive to α. Equations (9) and (17) imply

$$\theta_n(x_1)=i(4\pi\beta_0)^{-1/2}[\phi_{1,n}(x_1)+\phi_{2,n}(x_1)] , \tag{18}$$

so that

$$\psi^\dagger_{1,n}(x_1)\psi_{2,n}(x_1)+\text{H.c.} =(\pi\alpha)^{-1}\cos[(4\pi\beta_0)^{1/2}\theta_n(x_1)] . \tag{19}$$

To recover the $\cos\theta_n$ term of (6), the value $\beta_0=(4\pi)^{-1}$ is determined.

The magnetic-field term in (6) involves, by using Eqs. (17) and (18),

$$\partial\theta_n(x_1)/\partial x_1=(2\pi/L)\sum_q[\rho_{1,n}(q)+\rho_{2,n}(q)]\exp(-iqx_1), \tag{20}$$

which after x_1 integration and n summation is just the total fermion density. Since fluxons correspond to 2π variations in $\theta_n(x)$, Eq. (20) shows that each fluxon line at the nth layer corresponds to one fermion on the nth chain. The meandering of the flux line along the x_2 direction corresponds to the time evolution of the fermion.

The term with V_0 in (15) can be written as a free-fermion term by using the equivalence[29]

$$\sum_{q>0}[\rho_{1,n}(q)\rho_{1,n}(-q)+\rho_{2,n}(-q)\rho_{2,n}(q)] \leftrightarrow\sum_q q[a_n^\dagger(q)a_n(q)-b_n^\dagger(q)b_n(q)] , \tag{21}$$

which yields the final form of the fermion Hamiltonian,

$$\begin{aligned}\mathcal{H}_F=\sum_{n,q}\{&V_0 q[a_n^\dagger(q)a_n(q)-b_n^\dagger(q)b_n(q)]-\Delta_0[a_n^\dagger(q)b_n(q)+b_n^\dagger(q)a_n(q)]\\&-(H\phi_0/4\pi T)[a_n^\dagger(q)a_n(q)+b_n^\dagger(q)b_n(q)]+(2\pi/L)U_0\rho_{1,n}(q)\rho_{2,n}(-q)\}\\&+(\pi/L)\sum_{n\neq n'}\sum_q V_{n-n'}[\rho_{1,n}(q)+\rho_{2,n}(q)][\rho_{1,n'}(-q)+\rho_{2,n'}(-q)]\\&+(2\pi/L)\sum_{\pm}\sum_q(U_1-V_1)\rho_{1,n\pm1}(q)\rho_{2,n}(-q) ,\end{aligned} \tag{22}$$

where $\Delta_0=\pi J\alpha/\xi_0^2T$. The fermions $a_n(q)$ and $b_n(q)$ are now identified from the first term of (22) as right- and left-moving fermions with velocities $\pm V_0$, respectively. The Δ_0 term couples the right- and left-moving fermions and by itself would lead to a gap of $2\Delta_0$ in the spectrum. The magnetic-field term is a chemical potential which can create a finite fermion (or hole) density above (or below) the gap leading to a Fermi surface. All the other terms are density-density interactions, which from Eq. (11) and $\beta_0=(4\pi)^{-1}$ are

$$\begin{aligned}V_n&=\frac{T}{2\tau}\left[\left[2+\frac{d}{\lambda_e}\right]\delta_{n,0}-\delta_{n,\pm1}\right]+\frac{\tau}{2T}\frac{\lambda_e}{d}\left[1+\frac{4\lambda_e}{d}\right]^{-1/2}\alpha^{|n|} ,\\U_n&=V_n-\frac{T}{\tau}\left[\left[2+\frac{d}{\lambda_e}\right]\delta_{n,0}-\delta_{n,\pm1}\right] ,\end{aligned} \tag{23}$$

where

$$\alpha=1+d/2\lambda_e-(d/\lambda_e)^{1/2}(1+d/4\lambda_e)^{1/2} .$$

Since $U_n=V_n$ for all $n\neq1,0$, the only interchain interaction in (22) which involves U_n-V_n is that for neighboring chains with $U_1-V_1=T/\tau$ [the last term of (22)].

Note that for $\lambda_e/d\gg1$ the interactions (23) decay as $\exp[-|n|(d/\lambda_e)^{-1/2}]$, i.e., a decay which involves $(\lambda_e/d)^{1/2}\gg1$ layers. The magnitude of the interactions for $|n|\ll(\lambda_e/d)^{1/2}$ is $\sim(\lambda_e/d)^{1/2}\tau/4T$, which is comparable to the Fermi velocity V_0; i.e., Eq. (21) describes strongly interacting fermions. As shown in the next section, the magnetic-field term leads to different effective interactions between fermions near the Fermi surface for which a RG solution is possible.

The study in I, for $H=0$, shows that the fluxon system Eq. (6) has a phase transition at a temperature $T=T_f$ [Eq. (45) of I]. When $T<T_f$, the system has a finite correlation length ξ_f, which implies that the fermions in Eq. (22) have a gap $\Delta\sim\xi_f^{-1}$, i.e., Δ_0 is renormalized by the interactions into a finite Δ. Adding now the magnetic field means that when the corresponding chemical potential exceeds Δ, fermions start occupying states above the gap. In terms of fluxons, this phase transition is the critical field H_{c1} when fluxons start penetrating into the system, i.e., $H_{c1}=4\pi T\Delta/\phi_0$.

From the solution for ξ_f near T_f [Eq. (46) of I], H_{c1} has the form

$$H_{c1}\sim\exp[-b(1-T/T_f)^{-1/2}] , \tag{24}$$

where b is a constant, while not too close to T_f [Eq. (47) of I],

$$H_{c1}\sim\left[\frac{J}{T}\right]^{[2(1-T/\tau)]^{-1}} . \tag{25}$$

The RG method of I is not efficient for studying $H>H_{c1}$ since with a finite fluxon density $\theta_n(x)$ acquires

a term linear in x_1 whose Fourier transform is singular and its handling requires special care.[28] The present fermion approach is efficient for the range $T<T_f$ and $H>H_{c1}$, as demonstrated in the related commensurate-incommensurate problem.[25–27]

A qualitative understanding of the $H>H_{c1}$ case is obtained by a mean-field solution of (22) in which the order parameter is the fermion density n_f, i.e., $\langle \rho_{i,n}(q=0)\rangle = n_f/2$. This neglects another order parameter which is a density modulation with wave vector $2\pi n_f$. This modulation (whose onset is just the melting transition studied below) is assumed to be small compared with n_f; this is justified at least near the melting temperature and not too close to H_{c1}.

Assume in general that fluxons penetrate only every ℓth layer, where ℓ decreases with H. An ordered fluxon lattice has then periodicities $d\ell$ and n_f^{-1} in the directions perpendicular and parallel to the layers, respectively. Both n_f and ℓ are considered now as variational parameters. The on-chain terms of (22) correspond to fermions with dispersion $(\Delta_0^2+V_0^2q^2)^{1/2}$ on every ℓth chain with occupied states at $|q|<\pi n_f$. The interchain interactions are replaced by their $q=0$ terms and summed over all intervals $n-n'$ of occupied chains. The expectation value of (22) becomes

$$\frac{\langle H_F\rangle}{ML}=\int_0^{\pi n_f}\frac{dq}{\pi\ell}\left[(\Delta_0^2+V_0^2q^2)^{1/2}-\frac{H\phi_0}{4\pi T}\right] +\frac{\pi n_f^2\tau\lambda_e}{\ell Td}(1+4\lambda_e/d)^{-1/2}\frac{\alpha^\ell}{1-\alpha^\ell}+\frac{\pi}{2\ell}n_f^2U_0\ . \tag{26}$$

Minimizing (26) with respect to n_f and ℓ yields, for $1\ll\ell\ll(\lambda_e/d)^{1/2}$,

$$\tfrac{2}{3}\ell(\lambda_e/d)^{-1/2}(\pi V_0n_f/\Delta_0)^2\approx\ln(2\pi V_0n_f/\Delta_0)-\tfrac{1}{2}\ , \tag{27a}$$

$$H/H_{c1}\approx 4\pi V_0n_f(\lambda_e/d)^{1/2}/\Delta_0\ell\ , \tag{27b}$$

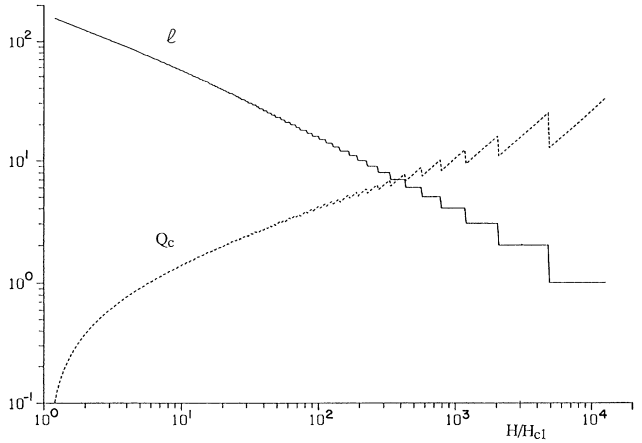

FIG. 1. Minima of the mean-field energy [Eq. (26)] for $\lambda_e/d=10^4$. The solid line is ℓ, and the dashed line is $Q_c=\pi V_0n_f/\Delta_0$, proportional to the fluxon-lattice wave vector parallel to the layers.

so that $\ell\sim H^{-2/3}$ and $n_f\sim H^{1/3}$ up to logarithmic terms. Note that for $\lambda_e/d\gg1$ the location of the minima of (26) is T independent.

Numerical results for minimizing (26) are shown in Fig. 1 for $\lambda_e/d=10^4$. The plateaus correspond to the range where a given ℓ has the lowest energy. Within a plateau, as H increases, the fluxon density increases only in the x_1 direction as shown by the increase in n_f (dashed curve). The centers of the plateaus are within 3% of Eq. (27) already for $\ell\geq4$; numerically fitted exponents are $\ell\sim H^{-0.61}$ and $n_f\sim H^{0.39}$.

The presence of a plateau for each integer ℓ is expected in general in view of the discreteness in ℓ; an ℓ phase is the stable phase for some range of fields. Similar conclusions were obtained by mean-field solutions of the original fluxon problem.[32,33]

III. MELTING TRANSITION

In this section, I derive the melting transition temperature $T_m^{(\ell)}$ of a fluxon lattice in an ℓ phase. The precise ℓ-H relation, as estimated above, is not essential for the following solution.

The melting transition is expected to be a second-order transition with a diverging correlation length at $T_m^{(\ell)}$ so that only low-lying excitations are relevant. In terms of fermions, the on-chain terms lead to occupation of fermion above a gap Δ with wave vectors $|q|<q_c$, while the interchain couplings may induce a gap at $\pm q_c$. The low-lying excitations are then electron-hole excitations near $\pm q_c$ which justify linearization of the spectrum near $\pm q_c$ with an appropriate new Fermi velocity; this procedure was efficient in solving the commensurate-incommensurate transition,[26] a problem which corresponds to the on-chain terms of (22).

The velocity term V_0 in (22) can be shifted to $V_0+U_0f_1$, and the added kinetic term is balanced by substracting a density-density interaction by using the equivalence (21); f_1 is, for now, arbitrary. The spectrum of the bilinear term is then $\pm E_q$ where $E_q=(\varepsilon_q^2+\Delta_0^2)^{1/2}$ and $\varepsilon_q=(V_0+U_0f_1)q$ so that q_c is given by $E_{q_c}=H\phi_0/4\pi T$. The velocity at the Fermi surface is then

$$V_c=(V_0+U_0f_1)^2q_c[(V_0+U_0f_1)^2q_c^2+\Delta_0^2]^{-1/2}\ . \tag{28}$$

Note that renormalization of q_c and V_c by interactions (e.g., as in the mean field solution of Sec. II) modifies the q_c-H relation; the following RG solution is however not sensitive to the precise values of these nonsingular corrections.

The next step is to define a Bogoliubov transformation to the fermion operators $\alpha_n(q),\beta_n(q)$ which diagonalize the bilinear terms, i.e.,

$$\begin{aligned} a_n(q)&=\gamma_q\alpha_n(q)-\delta_q\beta_n(q)\ ,\\ b_n(q)&=\delta_q\alpha_n(q)+\gamma_q\beta_n(q)\ , \end{aligned} \tag{29}$$

where $\gamma_q=[1+(E_q-\varepsilon_q)^2/\Delta_0^2]^{-1/2}$ and $\gamma_q^2+\delta_q^2=1$; for $H>H_{c1}$, the band of the $\alpha_n(q)$ fermions is partially occupied, while that of the $\beta_n(q)$ is full. Consider now an interaction term with the substitution of Eqs. (12) and (29):

$$\rho_{1,n}(q)\rho_{1,n'}(-q)=\sum_{p,p'}\gamma_{p+q}\gamma_p\gamma_{p'-q}\gamma_{p'}\alpha_n^\dagger(p+q)\alpha_n(p)\alpha_{n'}^\dagger(p'-q)\alpha_{n'}(p')+\cdots , \tag{30}$$

where terms with $\beta_n(q)$ operators are neglected. The latter terms describe excitations from a full band below the gap Δ and therefore do not contribute to low-energy excitations; these terms may shift the overall energy or even affect the dispersion of $\alpha_n(q)$. In the following RG solution, such interaction terms do not lead to logarithmic singularities and can therefore be neglected.

The next step is to focus on states near the Fermi surface $\pm q_c$ with velocities $\pm V_c$, where the precise value of q_c or V_c (being affected by the interactions) is not essential in the following. The interactions in Eq. (30) can be classified into small-q ones ($|q|\ll q_c$) and large-q ones ($q\approx\pm 2q_c$) which connect states $\alpha_n(p)\equiv\tilde{a}_n(p)$ for $p>0$ and $\alpha_n(p)\equiv\tilde{b}_n(p)$ for $p<0$. The new fermion operators $\tilde{a}_n(p)$ and $\tilde{b}_n(p)$ are relevant only near $\pm q_c$, respectively; hence, they can be considered as independent fermions for all p. The coefficients in (30) are replaced now by their values at $\pm q_c$, i.e.,

$$\begin{aligned}&\gamma_p\to\gamma_{q_c}\equiv\gamma_c,\quad \delta_p\to\delta_{q_c}\equiv\delta_c,\quad p>0 ,\\ &\gamma_p\to\gamma_{-q_c}\equiv\delta_c,\quad \delta_p\to\delta_{-q_c}\equiv\gamma_c,\quad p<0 ,\end{aligned} \tag{31}$$

so that (30) can be written as

$$\begin{aligned}\rho_{1,n}(q)\rho_{1,n'}(-q)\to&\gamma_c^4\tilde{\rho}_{1,n}(q)\tilde{\rho}_{1,n'}(-q)+\delta_c^4\tilde{\rho}_{2,n}(q)\tilde{\rho}_{2,n'}(-q)+2\gamma_c^2\delta_c^2\tilde{\rho}_{1,n}(q)\tilde{\rho}_{2,n'}(-q)\\&+2\gamma_c^2\delta_c^2\sum_{p,p'}\tilde{a}_n^\dagger(p+q)\tilde{b}_{n'}^\dagger(p'-q)\tilde{a}_{n'}(p')\tilde{b}_n(p) .\end{aligned} \tag{32}$$

The first three terms are density-density interactions with $\tilde{\rho}_{i,n}(q)$ defined as in Eq. (12) in terms of $\tilde{a}_n(p)$ and $\tilde{b}_n(p)$, and the last term is a backscattering interaction for the new fermions. Rewriting all the interaction terms of (22) in this manner yields an effective Hamiltonian for the low-lying excitations of the form

$$\begin{aligned}\tilde{\mathcal{H}}_F=&\sum_{n,q}V_c q[\tilde{a}_n^\dagger(q)\tilde{a}_n(q)-\tilde{b}_n^\dagger(q)\tilde{b}_n(q)]+(1/L)\sum_{n,n'}g_1(n-n')\sum_{p,p',q}\tilde{a}_n^\dagger(p+q)\tilde{b}_{n'}^\dagger(p'-q)\tilde{a}_{n'}(p')\tilde{b}_n^\dagger(p)\\&+(1/L)\sum_{n,n'}g_2(n-n')\sum_q\tilde{\rho}_{1,n}(q)\tilde{\rho}_{2,n'}(-q)+(1/2L)\sum_{n,n'}g_4(n-n')\sum_q[\tilde{\rho}_{1,n}(q)\tilde{\rho}_{1,n'}(-q)+\tilde{\rho}_{2,n}(q)\tilde{\rho}_{2,n'}(-q)] ,\end{aligned} \tag{33}$$

which has the conventional form of one-dimensional (1D) fermions[34] except that here the three types of couplings depend on chain indices. These couplings are

$$\begin{aligned}g_1(n)/2\pi&=2\gamma_c^2\delta_c^2(V_n+U_n) ,\\ g_2(n)/2\pi&=2\gamma_c^2\delta_c^2V_n+(\gamma_c^4+\delta_c^4)U_n ,\\ g_4(n)/2\pi&=(\gamma_c^4+\delta_c^4)V_n+2\gamma_c^2\delta_c^2U_n\\&\quad-(\gamma_c^4+\delta_c^4)(V_0+U_0f_1)\delta_{n,n'} .\end{aligned} \tag{34}$$

Here $g_1(n)$ is a backscattering interaction, $g_2(n)$ is a forward scattering of right- from left-moving fermions, and $g_4(n)$ is a forward scattering between right- (or left-) moving fermions.

The system (33) of electrons with interchain interactions has been studied in the context of phase transitions in one-dimensional chain systems[35–39] where electrons have interchain interactions. Of particular interest is the possibility of having a phase transition into a charge-density-wave (CDW) state; i.e., the fermion density becomes modulated with a wavelength of $(2q_c,k_c)$ (k_c depends on the interactions) and a gap opens at the Fermi surface. In terms of fluxons, a CDW corresponds to an ordered fluxon lattice with wave vectors $2q_c$ parallel to the layers and k_c perpendicular to them. The critical temperature for the onset of a CDW corresponds to the melting temperature of the fluxon lattice.

The RG solution of these type of problems[34] proceeds by identifying $\ln E_c/\omega$ terms in perturbation theory, where I follow here the procedure[40] in which ω/V_c and E_c/V_c are low and high cutoffs, respectively, in the momentum integrations. The relevant diagrams are shown in Fig. 2; each diagram involves integrations on internal Green's functions, as well as a dependence on

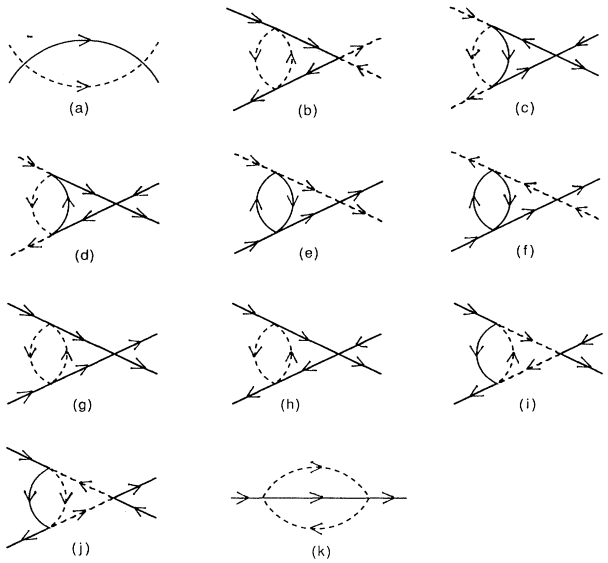

FIG. 2. Diagrams for the Hamiltonian (33). Solid and dashed lines correspond to right- and left-moving fermions, respectively. The value of each diagram is listed in Table II.

TABLE II. Diagrams. The graph column gives the figure label in Fig. 2 and the result of the integration in terms of $x=\ln E_c/\omega$; vortex column gives the type of vertex (Γ_i) or self-energy (Σ) being renormalized by the terms in the contribution column. Note that two-loop terms lead to distinct diagrams when right- and left-moving fermions are interchanged so that an additional factor of 2 should be included.

Graph	Vertex	Contributions
(a) x	Γ_1	$-2\gamma_1(n-n')\gamma_2(n-n')-\sum_m \gamma_1(n-m)\gamma_1(m-n')+2\gamma_1(n-n')\gamma_2(0)$
	Γ_2	$-\gamma_1^2(n-n')$
(b) $x/2$	Γ_1	$-4\gamma_1(n-n')\sum_m \gamma_2(n-m)\gamma_2(m-n')+2\gamma_1(n-n')\gamma_1(0)\gamma_2(n-n')$
	Γ_2	$-2\gamma_1^2(n-n')\gamma_1(0)+2\sum_m \gamma_1^2(n-m)\gamma_2(m-n')-4\gamma_1(0)\gamma_2(0)\gamma_2(n-n')$ $+2\gamma_2(n-n')\sum_m \gamma_2^2(m)$
(c) $x/2$	Γ_1	$2\gamma_1(n-n')\gamma_2(n-n')\gamma_4(n-n')$
	Γ_2	$2\gamma_1(0)\gamma_2(0)\gamma_4(n-n')+\gamma_2^2(n-n')\gamma_4(0)$ $-\sum_m \gamma_4(n-m)\gamma_2^2(m-n')+\gamma_1^2(n-n')\gamma_4(0)-\sum_m \gamma_1^2(n-m)\gamma_4(m-n')$
(d) $x/2$	Γ_1	$\gamma_4(n-n')\sum_m \gamma_1(n-m)\gamma_1(m-n')-2\gamma_1(n-n')\gamma_2(0)\gamma_4(n-n')$
	Γ_2	$\gamma_4(n-n')\sum_m \gamma_1^2(m)-2\gamma_1(0)\gamma_2(0)\gamma_4(n-n')-\gamma_2^2(n-n')\gamma_4(0)$ $+\sum_m \gamma_4(n-m)\gamma_2^2(m-n')$
(e) $-x/2$	Γ_1	$-2\gamma_1(n-n')\sum_m \gamma_2(n-m)\gamma_4(m-n')+2\gamma_1(n-n')\gamma_1(0)\gamma_4(n-n')$ $+2\gamma_1(n-n')\gamma_2(n-n')\gamma_4(0)+2\gamma_1(n-n')\gamma_2(n-n')\gamma_4(n-n')$
	Γ_2	$-2\gamma_2(n-n')\sum_m \gamma_4(n-m)\gamma_2(m-n')+2\gamma_1(0)\gamma_2(n-n')\gamma_4(n-n')$ $-2\gamma_2^2(n-n')\gamma_4(0)+2\gamma_1^2(n-n')\gamma_4(n-n')$
(f) $-x/2$	Γ_1	$2\gamma_1(n-n')\sum_m \gamma_2(m)\gamma_4(m)-2\gamma_1(n-n')\gamma_1(0)\gamma_4(0)-2\gamma_1(n-n')\gamma_2(0)\gamma_4(0)$ $-2\gamma_1(n-n')\gamma_2(0)\gamma_4(n-n')+2\sum_m \gamma_1(n-m)\gamma_4(n-m)\gamma_1(m-n')$
	Γ_2	$2\gamma_2(n-n')\sum_m \gamma_4(n-m)\gamma_2(m-n')-2\gamma_1(0)\gamma_2(n-n')\gamma_4(n-n')$ $+2\gamma_2^2(n-n')\gamma_4(0)$
(g) $x/2$	Γ_4	$2\gamma_4(n-n')\sum_m \gamma_2(n-m)\gamma_2(m-n')+4\gamma_1(0)\gamma_2(n-n')\gamma_4(n-n')$ $+2\gamma_2^2(n-n')\gamma_4(n-n')$
(h) $x/2$	Γ_4	$-2\gamma_4(n-n')\sum_m \gamma_2(n-m)\gamma_2(m-n')-4\gamma_1(0)\gamma_2(n-n')\gamma_4(n-n')$ $-2\gamma_1^2(n-n')\gamma_4(0)+2\gamma_4(n-n')\sum_m \gamma_2^2(m)-4\gamma_1(0)\gamma_2(0)\gamma_4(n-n')$ $+2\sum_m \gamma_1^2(n-m)\gamma_4(m-n')$
(i) $x/2$	Γ_4	$2\gamma_1(n-n')\sum_m \gamma_1(n-m)\gamma_1(m-n')-4\gamma_1^2(n-n')\gamma_2(0)-2\gamma_1(0)\gamma_2^2(n-n')$ $+2\gamma_1(0)\gamma_2^2(n-n')-4\gamma_1(0)\gamma_2(0)\gamma_2(n-n')+2\sum_m \gamma_2^2(n-m)\gamma_2(m-n')$
(j) $x/2$	Γ_4	$4\gamma_1^2(n-n')\gamma_2(n-n')+4\gamma_1(0)\gamma_2(0)\gamma_2(n-n')+2\gamma_1(0)\gamma_2^2(n-n')$ $-2\sum_m \gamma_2^2(n-m)\gamma_2(m-n')+2\gamma_1(0)\gamma_1^2(n-n')-2\sum_m \gamma_1^2(n-m)\gamma_2(m-n')$
(k) $x/2$	Σ	$-\sum_m \gamma_1^2(m)-\sum_m \gamma_2^2(m)+2\gamma_1(0)\gamma_2(0)$

$g_i(n-n')$ $(i=1,2,4)$. The integrations are fairly standard[34,40] with the results collected in the first column of Table II where $x=\ln E_c/\omega$. The dependence on $g_i(n-n')$ is found by decomposing each vertex (with four legs) in the diagram to all possible distinct diagrams with pairs of two legs; each such decomposed diagram determines a particular product of the $g_i(n-n')$. The result of this decomposition is given in Table I, separating them into the various renormalized vertices Γ_i, corresponding to $\gamma_i(n-n')=g_i(n-n')/2\pi V_c$, and to a self-energy Σ.

The RG equations are generated[34] by the $\ln E_c/\omega$ coefficients of $\Gamma_i\Sigma^2$. Considering first the one-loop result, the renormalized couplings satisfy

$$\frac{\partial\gamma_1(n-n',x)}{\partial x}=-\sum_m \gamma_1(n-m,x)\gamma_1(m-n',x) -2\gamma_1(n-n',x)[\gamma_2(n-n',x)-\gamma_2(0,x)] ,$$
$$\frac{\partial\gamma_2(n-n',x)}{\partial x}=-\gamma_1^2(n-n',x) . \tag{35}$$

In terms of the Fourier-transformed $\gamma_i(k,x)=\sum_n\gamma_i(n,x)\exp(ikn)$ $(i=1,2,4)$, these equations become

$$\frac{\partial\gamma_1(k,x)}{\partial x}=-\gamma_1^2(k,x) -\frac{2}{M}\sum_{k'}\gamma_2(k')[\gamma_1(k-k',x)-\gamma_1(k,x)] , \tag{36a}$$

$$\frac{\partial\gamma_2(k,x)}{\partial x}=-\frac{1}{M}\sum_{k'}\gamma_1(k-k',x)\gamma_1(k',x) . \tag{36b}$$

Since $\gamma_1(n=0,x)$ is equivalent to $-\gamma_2(n=0,x)$ by interchanging the ordering of fermion operators, one can add a k-independent term to both $\gamma_1(k,x)$ and $\gamma_2(k,x)$ without affecting the result. This feature can be used to shift the initial $\gamma_1(k,0)$ so that $\gamma_1(k,0)\geq 0$ for all $|k|\leq\pi$.

From Eqs. (11) and (34), the initial values become

$$\gamma_1(k,0)=(8\pi\gamma_c^2\delta_c^2/V_c)[\beta(k)-\beta(\pi)] ,$$
$$\gamma_2(k,0)=(1/V_c)\{2\pi\beta(k)-(\gamma_c^2-\delta_c^2)^2/[8\pi\beta(k)] -8\pi\gamma_c^2\delta_c^2\beta(\pi)\} . \tag{37}$$

For $\lambda_e/d\gg 1$, $\gamma_1(k,0)$ is sharply peaked at $k=0$ and then decreases slowly to $\gamma_1(\pi,0)=0$. The onset of a CDW is signaled by an appearance of a negative $\gamma_1(k,x)$ at some k, which then diverges[37,39] to $-\infty$. The most susceptible k for this scenario is at the minimum of $\gamma_1(k,0)$, i.e., at $k=\pi$; this would yield a triangular fluxon lattice. Thus, if the initial flow of $\gamma_1(k,x)$ is into a negative value, the $-\gamma_1^2(k,x)$ term in (36a) will eventually yield the divergence to $-\infty$.

The initial flow of $\gamma_1(\pi,x)$ is dominated by $k'\approx\pi$ in Eq. (36a), i.e., by the sign of $\gamma_2(\pi,0)$, where

$$\gamma_2(\pi,0)=[8\pi V_c\beta(\pi)]^{-1}(\gamma_c^2-\delta_c^2)^2\{[4\pi\beta(\pi)]^2-1\} . \tag{38}$$

The sign of (38) is negative for $T<\tau/4$, which remarkably is independent of H (the latter affecting γ_c, δ_c, and V_c). Note that the RG expansion in γ_1 is valid near $k=\pi$ and $T=\tau$ since both $\gamma_i(k\approx\pi,0)$ $(i=1,2)$ are small. Thus the scenario for $T<\tau/4$ is consistent and the system is unstable. For $T>\tau/4$, $\gamma_1(\pi,x)$ initially increases so that $\gamma_1(k,x)$ has a weaker k dependence and presumably becomes k independent when $x\to\infty$, corresponding to a gapless or disordered phase. The latter case, however, depends also on the behavior of $\gamma_1(k,x)$ at $k\neq\pi$, where it is not small and higher-order terms in γ_1 can affect the trajectories. Thus $\tau/4$ is a lower bound for the melting temperature $T_m^{(1)}$.

For an ℓ phase, fermions are present only on every ℓth chain so that the initial couplings are

$$\gamma_{i,\ell}(k,0)=\sum_n\gamma_i(n\ell,0)\exp(ikn\ell) =(1/\ell)\sum_{m=0}^{\ell-1}\gamma_i(k+2\pi m/\ell,0) . \tag{39}$$

Repeating the previous analysis yields now an instability when

$$T<\tfrac{1}{4}\tau\sum_m \sin^{-2}[\pi(2m+1)/2l]/\sum_m \sin^2[\pi(2m+1)/2l] , \tag{40}$$

which yields the lower bounds on the melting temperatures,

$$T_m'^{(\ell)}=\tau/4,\quad \ell=1;\quad T_m'^{(\ell)}=\tau\sqrt{\ell/8},\quad \ell\geq 2 . \tag{41}$$

Note that for large H, $H\gg H_{c1}$, the mixing in (29) should be small, e.g., in mean field $\delta_c^2\approx(H_{c1}/H)^{2/3}\ll 1$. Thus the backscattering coupling $\gamma_1(k,0)$ of Eq. (37) is small for $H\gg H_{c1}$ even near $k=0$; $\gamma_2(k\approx 0,0)$ is however of order 1. It turns out that $\gamma_1(k,x)$ appears in first order in both one and two loop levels (see Table II) but only in second order in three loop level.[40] Thus for $H\gg H_{c1}$ it is necessary *and* sufficient to consider RG with two loops. Note that $H\gg H_{c1}$ corresponds to a fairly large range of ℓ values, e.g., $\ell<60$ in Fig. 1 for $H/H_{c1}>10$.

I proceed now to the two-loop equations and their numerical solution. The two-loop terms in Table II (which now involve γ_4) in terms of $\gamma_i(k)$ (x is implicit for brevity) lead to the following RG equations:

$$\frac{\partial\gamma_1(k)}{\partial x}=-\gamma_1^2(k,x)-\frac{2}{M}\sum_{k'}\gamma_2(k')[\gamma_1(k-k')-\gamma_1(k)][1+\bar{\gamma}_1+\bar{\gamma}_4]$$
$$-\gamma_1(k)\frac{1}{M}\sum_{k'}[\gamma_1^2(k')+\gamma_2^2(k')+2\gamma_2(k')\gamma_4(k')]$$
$$+\frac{1}{M}\sum_{k'}[\gamma_1(k')\gamma_2^2(k-k')+2\gamma_1(k')\gamma_2(k-k')\gamma_4(k-k')+\gamma_4(k')\gamma_1^2(k-k')]$$
$$-\frac{2}{M}\sum_{k'}\gamma_1(k')\gamma_4(k-k')\bar{\gamma}_1-\gamma_1(k)\frac{2}{M}\sum_{k'}\gamma_1(k')\gamma_4(k-k')+2\gamma_1(k)\bar{\gamma}_1\bar{\gamma}_4\ , \tag{42a}$$

$$\frac{\partial\gamma_2(k)}{\partial x}=-\frac{1}{M}\sum_{k'}\gamma_1(k')\gamma_1(k-k')[1+\bar{\gamma}_1-\bar{\gamma}_4]-\frac{2}{M^2}\sum_{k',k''}\gamma_1(k')\gamma_1(k'')\gamma_4(k-k'-k'')$$
$$-[\gamma_2(k)-\gamma_4(k)]\frac{1}{M}\sum_{k'}\gamma_1(k')[\gamma_1(k')-\gamma_1(k-k')]\ , \tag{42b}$$

$$\frac{\partial\gamma_4(k)}{\partial x}=-\frac{\partial\gamma_2(k)}{\partial x}-\frac{1}{M}\sum_{k'}\gamma_1(k')\gamma_1(k-k')[1+2\bar{\gamma}_2]$$
$$+\frac{1}{M^2}\sum_{k',k''}\gamma_1(k')\gamma_1(k'')[2\gamma_2(k-k'-k'')-\gamma_4(k-k'-k'')]+\frac{1}{M}\sum_{k'}\gamma_1(k')\gamma_1^2(k-k')\ . \tag{42c}$$

These results extend those of Ref. 37 to include the γ_4 terms [note a misprint in the sign of the last term in Eq. (16) of Ref. 37].

In the following I choose f_1 in Eq. (28) so that $g_4(n=0)=0$ [Eq. (34)]; this choice eliminates the ambiguity in cutoff procedures[41] associated with two identical fermions at short range. Thus

$$f_1=2\gamma_c^2\delta_c^2/(\gamma_c^4+\delta_c^4)=(1-a_c)/(1+a_c)\ , \tag{43}$$

where $a_c=1-4\gamma_c^2\delta_c^2$. Equation (28) then becomes

$$V_c=[V_0+U_0(1-a_c)/(1+a_c)]\sqrt{a_c}\ . \tag{44}$$

The parameters involved in Eq. (42) are T/τ, λ_e/d, and a_c, with the latter one depending on H. For example, from the mean-field estimate Eq. (27b) for $\ell\ll(\lambda_e/d)^{1/2}$ (i.e., H is not too close to H_{c1})

$$1-a_c\approx 4\ell(d/\lambda_e)^{1/2}\approx(H_{c1}/H)^{2/3}\ll 1\ .$$

The initial values can be written in the form

$$\gamma_1(k,0)=(2\pi/V_c)(1-a_c)\beta(k)\ ,$$
$$\gamma_2(k,0)=(1/8\pi V_c)[16\pi^2\beta(k)-a_c/\beta(k)]\ , \tag{45}$$
$$\gamma_4(k,0)=(1/8\pi V_c)[16\pi^2\beta(k)+a_c/\beta(k)-4\pi(1+a_c)(V_0+U_0f_1)]\ .$$

For an ℓ phase, the forms (45) are substituted in Eq. (39) and then used as initial conditions. [Note that in Eq. (37), $\gamma_1(\pi,0)$ was subtracted.]

In view of the sharp structure in $\gamma_i(k)$, numerical solutions for large λ_e/d involve many chains, i.e., a large number of coupled differential equations. Since the instability occurs in $\gamma_1(k)$, the RG equation for $\gamma_4(k)$ [Eq. (42c)] can be neglected as it yields higher-order corrections for the other equations. [In fact, the numerical solution shows that $\gamma_4(k)$ is hardly affected by the RG.] Thus $\gamma_4(k,0)$ is used in Eqs. (42a) and (42b).

Some examples are presented in Figs. 3–6 for $\lambda_e/d=10^4$; the number of chains required for convergence was $M=960$ for $\ell=1$ and $M=240$ for $\ell=15$; the $\ell=15$ case was also studied for $\lambda_e/d=10^6$ with $M=960$. The numerical solutions show in general that the initial sharp structure of $\gamma_i(k,0)$ is flattened rapidly; the weak structure that remains eventually produces an instability at low T/τ. The instability wave vector approaches π with increasing T/τ and equals π in some interval until a critical temperature $T_m''^{(\ell)}$. Above $T_m''^{(\ell)}$, the initial flattening of $\gamma_1(k,x)$ is somewhat more rapid and, at large x, $\gamma_1(k,x)$ becomes completely flat. These features are illustrated in Fig. 3 for $\ell=5$ and in Fig. 4 for $\ell=15$. The values of a_c are chosen to correspond to the plateaus in the mean-field calculation (Fig. 1); however, $T_m''^{(\ell)}$ was found to be insensitive to the choice of a_c, i.e., to variations in H. The dependence on H is indirect via the dependence of ℓ on H. For example, for $\ell=15$ variations in the parameter $(1-a_c)^{-1/2}$ from 1.5 to 3 change $T_m''^{(\ell)}$ by 6%, while a further increase to 10^3 (keeping formally $\ell=15$) did not affect $T_m''^{(\ell)}$ within the numerical resolution of 1%; this corresponds roughly to H/H_{c1} varying from ~ 3 to 30 and then to 10^9. Thus the precise location of an ℓ phase in terms of H is not significant for determining the critical temperature. Furthermore, $T_m''^{(\ell)}$ is insensitive to the value of λ_e/d as long as $\ell\ll(\lambda_e/d)^{1/2}$. For example, $T_m''^{(15)}$ varies by $\sim 1\%$ when λ_e/d varies from 10^4 to 10^6. Note also that the coupling $\gamma_2(k)$ is weakly affected by the RG, as illustrated in Fig. 5.

Table III summarizes the numerical data for $T_m''^{(\ell)}$; as expected, these are higher than the lower bounds of Eq. (41). It is reasonable to expect that $T_m''^{(\ell)}$ is an upper bound on the exact $T_m^{(\ell)}$; at $T>T_m''^{(\ell)}$, $\gamma_1(k,x)$ becomes flat and the weak-coupling scheme becomes valid. In fact, the one-loop calculations give higher values of $T_m''^{(\ell)}$

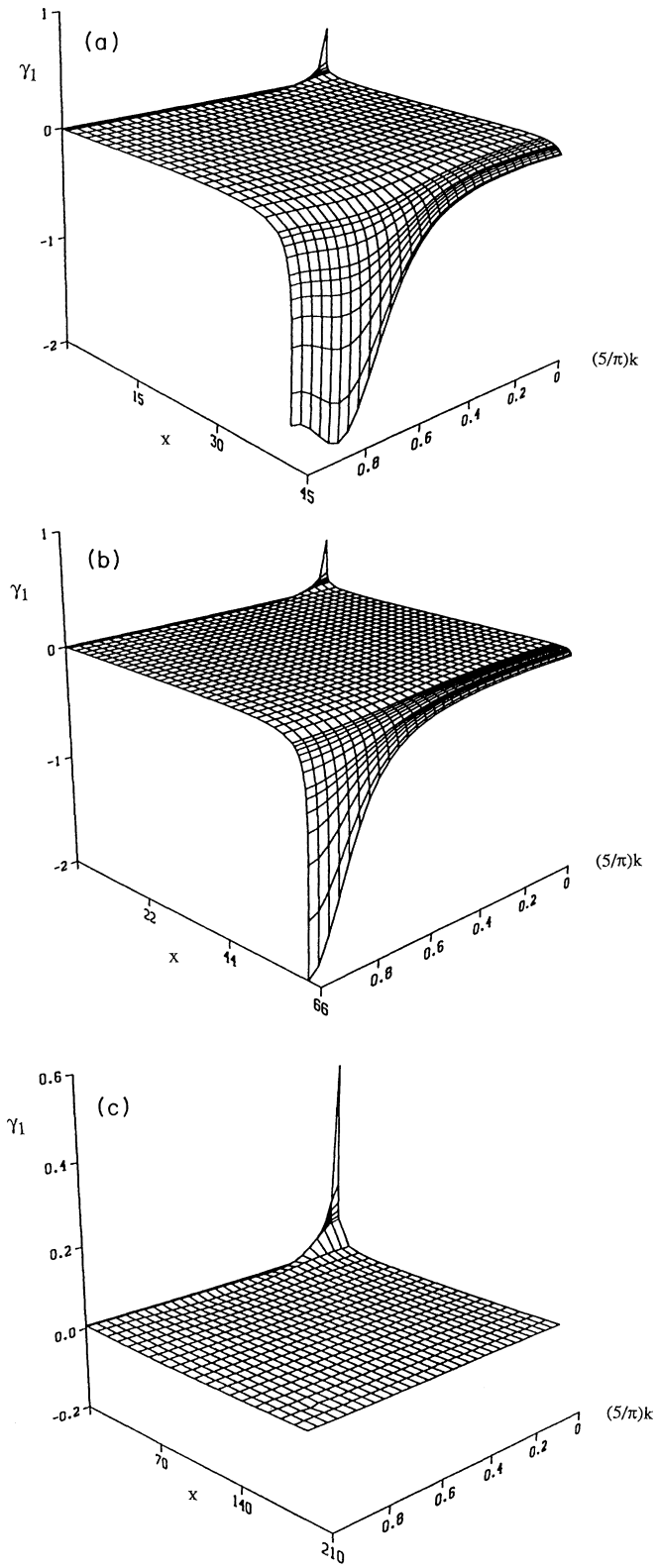

FIG. 3. RG trajectory of Eq. (42) for $\gamma_1(k,x)$ with $\ell=5$, $\lambda_e/d=10^4$ and $(1-a_c)^{-1/2}=8.7$; the latter value corresponds to the $\ell=5$ plateau in Fig. 1 and is $\approx(H/H_{c1})^{1/3}$ in the mean-field estimate of Eq. (27). (a) $T/\tau=0.7$, (b) $T/\tau=0.8$, and (c) $T/\tau=0.9$. The melting temperature of this case is $T_m''^{(5)}=0.89$.

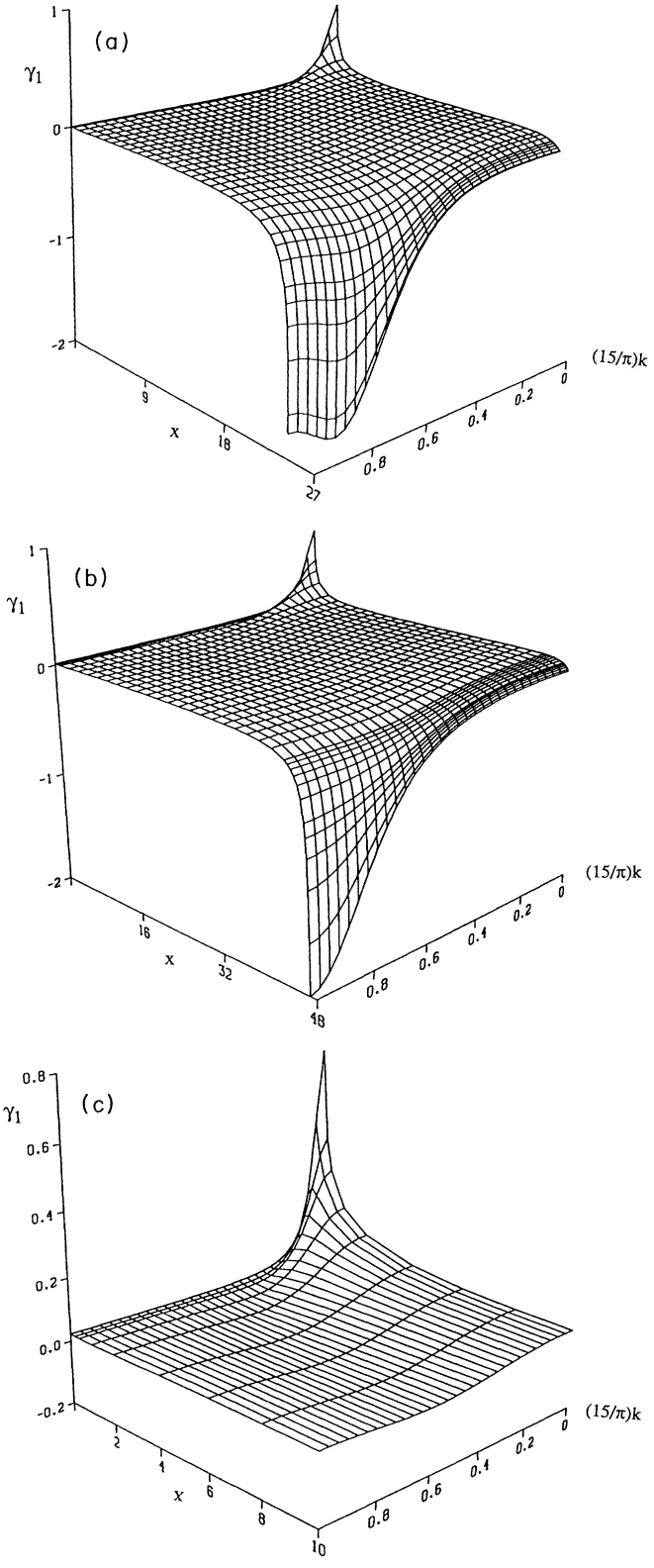

FIG. 4. Same as Fig. 3 with $\ell=15$ and $(1-a_c)^{-1/2}=4.1$. (a) $T/\tau=1.4$, (b) $T/\tau=1.5$, and (c) $T/\tau=1.6$. In (c) only the initial trajectory is shown, demonstrating the rapid initial flattening of $\gamma_1(k,x)$; at large x, $\gamma_1(k,x)$ becomes completely flat. The melting temperature of this case is $T_m''^{(15)}=1.55$.

TABLE III. Critical temperatures. The vortex transition temperature $T_v^{(\ell)}$, the lower bound on the melting temperature $T_m'^{(\ell)}$ [Eq. (41)], and the numerical results of the RG equations $T_m''^{(\ell)}$.

ℓ	$T_v^{(\ell)}/\tau$	$T_m'^{(\ell)}/\tau$	$T_m''^{(\ell)}/\tau$
1	0.12	0.25	0.36
2	0.25	0.5	0.55
3	0.37	0.61	0.69
4	0.5	0.71	0.80
5	0.62	0.79	0.89
6	0.75	0.87	0.98
7	0.87	0.94	1.06
8	1.0	1.0	1.13
9	1.12	1.06	1.20
10	1.25	1.12	1.27
11	1.37	1.17	1.33
12	1.5	1.22	1.39
13	1.62	1.27	1.44
14	1.75	1.32	1.50
15	1.87	1.37	1.55

so that results from a higher-loop calculation approach $T_m^{(\ell)}$ from above.

It is interesting to compare the $\ell=1$ result with the asymptotic high-field limit of Korshunov and Larkin,[23] $T_m^{(1)}/T_v^{(1)}=\frac{8}{3}$. Since $T_v^{(1)}=\tau/8$, the data from Table III yield $T_m^{(1)}/T_v^{(1)}=2.88$, i.e., an 8% difference. Thus indeed $T_m''^{(1)}$ is an upper bound and is fairly close to the exact high-field result.

The upper and lower bounds are summarized in Table III and plotted in Fig. 6. The closeness of $T_m''^{(\ell)}$ and $T_m'^{(\ell)}$ suggests that the exact $T_m^{(\ell)}$ varies as $\sqrt{\ell}$, as in Eq. (41). The full phase digram is shown in Fig. 7, assuming the mean-field results in Fig. 1 for the magnetic-field range of an ℓ phase.

IV. VORTEX-FLUXON COMPETITION

In this section the full problem of Eq. (15) of I is considered, i.e., the effect of in-layer vortex fluctuations on the melting temperature. In an ℓ phase, fluxons penetrate only between groups of ℓ neighboring layers; the layers in each group are phase correlated both above and below $T_m^{(\ell)}$ and can be considered as an effective layer. For $T<T_m^{(\ell)}$ fluxons have positional long-range order and all layers are correlated, while for $T>T_m^{(\ell)}$ fluxon

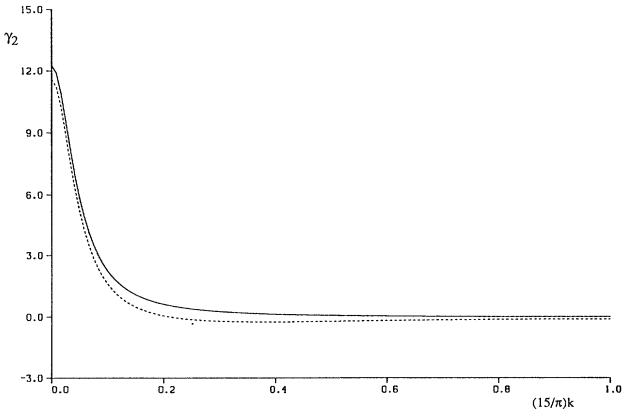

FIG. 5. RG behavior of $\gamma_2(k,x)$ corresponding to the case of Fig. 4(b). The solid line is the initial value at $x=0$, and the dashed line is at $x=47$ near which $\gamma_1(k,x)$ becomes unstable.

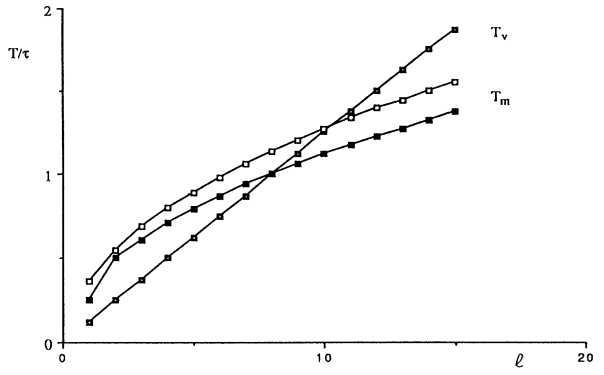

FIG. 6. Critical temperatures for $T_v^{(\ell)}/\tau$ (straight line) and for the upper and lower bounds on the melting temperature $T_m^{(\ell)}/\tau$ (curved lines).

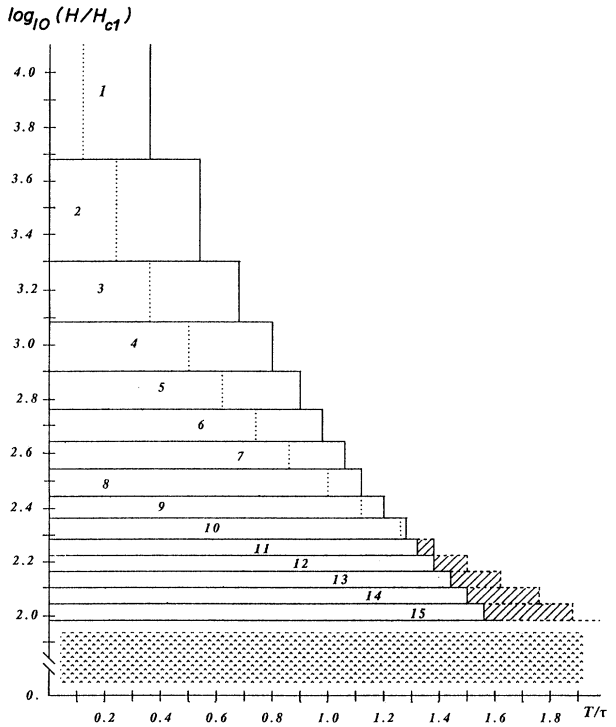

FIG. 7. Phase diagram of the ℓ phases. The H/H_{c1} values use the plateaus of Fig. 1. Solid vertical lines are the melting temperatures $T_m^{(\ell)}/\tau$ (taking here the numerical results $T_m''^{(\ell)}/\tau$); dotted vertical lines are for $T_v^{(\ell)}/\tau$ which satisfy $T_v^{(\ell)}/\tau<T_m^{(\ell)}/\tau$, i.e., no 2D phases. Dashed vertical lines are for $T_v^{(\ell)}/\tau$ which satisfy $T_v^{(\ell)}/\tau>T_m^{(\ell)}/\tau$ and are therefore strict 2D transitions. The shaded areas are 2D phases. The 2D ℓ phases continue into the patterned area until $T_m^{(\ell)}$ approaches T_c.

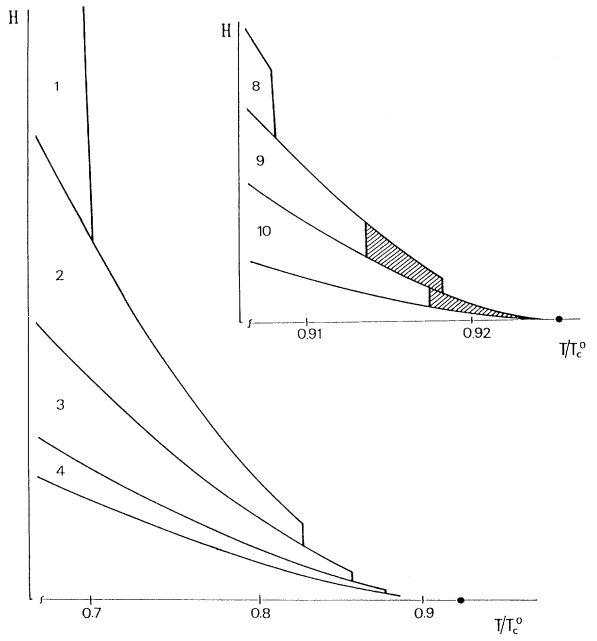

FIG. 8. H-T phase diagram by allowing $\tau(T)$ dependence and $H_{c1}(T)$ from Eq. (24). Vertical phase boundaries are 3D transitions for $\ell=1-4$. The inset shows the region closer to T_c with two transitions when $T_v^{(\ell)}/\tau > T_m^{(\ell)}/\tau$; the shaded areas are 2D phases for $\ell=9,10$. The temperature scale corresponds to $T_c^0/\tau_0=0.1$ and $T_c/\tau=1.23$. $T_c/T_c^0=0.925$ is marked by a solid circle. The field scale can be estimated from Fig. 1.

fluctuations decouple the effective layers.

This scenario leads to the problem of the phase transition in a system with a finite number of layers. This was studied by Monte Carlo simulations[24] in the limit of an X-Y model, i.e., $\lambda_e/d\to\infty$; the results show that for small ℓ the vortex transition $T_v^{(\ell)}$ increases rapidly and then saturates at the 3D critical temperature T_c. If $T_v^{(\ell)}$ is not too close to T_c, the dominant fluctuations are those of vertical vortex lines; i.e., vortex points on different layers are position correlated to form a line. This implies that ℓ layers act as an effective single layer so that $T_v^{(\ell)}=(\tau/8)\ell$ [Eq. (3)]. As ℓ increases, $(\tau/8)\ell$ becomes too close to T_c in the sense that the 3D correlation length $\xi^{3D}(T)$ at $T=(\tau/8)\ell$ is shorter than the thickness $d\ell$ of the layer. In the latter case, the dominant critical fluctuations are vortex loops.[24]

For the conventional X-Y model, $T_c/T_v^{(1)}=2.4$ so that, already for $\ell=2$, $\tau/4$ is fairly close to T_c; even so, the simulations show that[24] $T_v^{(2)}/T_v^{(1)}\approx 1.6$; i.e., the initial rise with ℓ is steep. In the companion paper, I have shown that T_c is a sensitive function of the vortex-core energy E_c. When E_c is moderately large, so that $\exp(-E_c/\tau)\ll J/T_c\lesssim 1$, $T_c/\tau>1$ is possible so that the variation in $T_v^{(\ell)}$ as ℓ increases can be larger than 8.

It is therefore possible, at least in principle, that $T_v^{(\ell)}=(\tau/8)\ell$ for $\ell>8$. In fact experimental data on well separated $YBa_2Cu_3O_7$ layers[42] show that T_v increases from 71 K for 3 bilayers ($\ell=6$) to 80 K for $\ell=8$ and to 87 K for $\ell=16$. More recent data[43] show that T_v increases with thickness up to 60 Å ($\ell\approx 10$) with T_c^0 fairly constant. Since $\tau(T)$ decreases as T approaches T_c^0, the ratio $T_v/\tau(T_v)$ can be linear with ℓ (as discussed in Sec. VI of I) even at $\ell=16$. The values $(\tau/8)\ell$ are included in Table III and in Fig. 6.

As shown in Table III and Fig. 6, $T_v^{(\ell)}>T_m^{(\ell)}$ for $\ell>\ell_{\min}$, where $\ell_{\min}$ is between 8 and 10, corresponding to the lower and upper bounds on $T_m^{(\ell)}$. The possibility $T_v^{(\ell)}>T_m^{(\ell)}$ allows for 2D phases; i.e., in the range $T_m^{(\ell)}<T<T_v^{(\ell)}$ vortices are not thermally excited while the fluxon lattice has melted. Thus the effective layers in an ℓ phase are decoupled from each other by thermal fluctuations and exhibit 2D behavior in a strict sense. This scenario was also proposed in analogy with dislocation theory,[44] though the condition $T_v^{(\ell)}>T_m^{(\ell)}$ was assumed with no proof.

As ℓ increases, $T_m^{(\ell)}$ must saturate at T_c and then 2D phases are not possible. Thus, for $\ell>\ell_{\max}$, where $T_m^{(\ell)}$ is too near to T_c, 2D phases do not exist. As discussed above, $\ell_{\max}$ depends sensitively on the model parameters E_c and J. The full phase diagram in the H-T plane is shown in Fig. 7.

Finally, note that τ is itself temperature dependent in a superconductor; assuming $\lambda_{ab}=\lambda'(1-T/T_c^0)^{-1/2}$ yields $\tau=\tau_0(1-T/T_c^0)$ with τ_0 typically 10^3-10^4 K. Assuming a critical temperature of $T_c/\tau(T_c)=1.23$ (see Fig. 6 of I) and allowing for $H_{c1}(T)$ as in Eq. (24) yields the phase diagram of Fig. 8, assuming $\ell_{\min}=8$. The shaded areas are 2D phases with $\ell=9,10$. An increase in T_c/τ due to either higher J or higher core energy E_c (Fig. 6 of I) generates additional 2D phases with $\ell>10$.

V. DISCUSSION

The data in Table I show that $r_{\max}\gg r_J$; i.e., the experimentally observed relation (2) corresponds to unbinding of vortices at distances where the Josephson coupling should dominate. The limit on $r_{\max}$ is the experimental resolution and sample size; depending on the sample and temperature, $r_{\max}/r_J$ varies between 10 and 10^2. To account for such data, one must assume that the value of J, as extrapolated from low-temperature data, must be strongly renormalized by thermal fluctuations.

A second remarkable experimental result are the values 6–14 of ℓ_{eff}; this can be related to the ℓ phases of the present work. A third relevant observation is the large variation of T_c in superlattices when J is reduced by introducing nonsuperconducting material (see Sec. VI of I). The latter effect indicates that J is not small, which seems inconsistent with the presence of 2D phenomena.

All three pieces of this puzzle hang together if in the experiment there is some (unintentional or unspecified) magnetic field parallel to the layers. In fact, data with weak magnetic fields perpendicular to the layers[11] show a significant reduction in the exponent $a(T)$ [Eq. (2)]. This can be understood if the magnetic field has a small component parallel to layers; as this component increases, ℓ is decreased and therefore $a(T)\sim\ell$ is reduced. From the mean-field estimate, $a(T)\sim H^{-0.6}$, which is consistent

with the data.

The presence of Eq. (2) for high fields and well below T_c (Refs. 10, 12, and 13) seems outside the range of strict 2D phases. It is possible that J is reduced by thermal fluctuations, but remains finite, so that Eq. (2) can be valid for not too small currents.

In conclusion, the present work has studied the melting transition of an ℓ phase. The solution is of interest for the general phenomena of melting transitions as well as for understanding a number of puzzling experiments.

ACKNOWLEDGMENTS

I am grateful to A. I. Larkin, S. E. Korshunov, S. N. Artemenko, D. Baeriswyl, L. Bulaevskii, and D. C. Mattis for most valuable discussions. I thank the Institute for Scientific Interchange in Villa Gualino, Torino, for their hospitality while part of this work was done. This research was supported by the Basic Research Foundation administered by the Israel Academy of Sciences and Humanities.

[1]S. N. Artemenko, I. G. Gorlova, and Yu. I. Latyshev, Phys. Lett. **138**, 428 (1989); Pis'ma Zh. Eksp. Teor. Fiz. **49**, 566 (1989) [JETP Lett. **49**, 654 (1989)]; S. N. Artemenko and Yu. I. Latyshev, Mod. Phys. Lett. B **6**, 367 (1992).

[2]D. H. Kim, A. M. Goldman, J. H. Kang, and R. T. Kampwirth, Phys. Rev. B **40**, 8834 (1989).

[3]N.-C. Yeh and C. C. Tsuei, Phys. Rev. B **39**, 9708 (1989).

[4]Q. Y. Ying and H. S. Kwok, Phys. Rev. B **42**, 2242 (1990).

[5]H. Teshima, K. Ohata, H. Izumi, K. Nakao, and T. Morishita, Physica C **185-189**, 1865 (1991); C. Paracchini, L. Romano, and L. Francesio, *ibid.* **175**, 324 (1991).

[6]S. Q. Chen, W. J. Skocpol, E. DeObaldia, M. O'Malley, and P. M. Mankiewich (unpublished).

[7]S. Vadlamannati, Q. Li, T. Venkatesan, W. L. McLean, and P. Lindenfeld, Phys. Rev. B **44**, 7094 (1991).

[8]S. Martin, A. T. Fiory, G. P. Espinosa, and A. S. Cooper, Phys. Rev. Lett. **62**, 677 (1989).

[9]V. A. Gasparov, Physica C **178**, 449 (1991).

[10]T. Onogi, T. Ichiguchi, and T. Aida, Solid State Commun. **69**, 991 (1989); M. Ban, T. Ichiguchi, and T. Onogi, Phys. Rev. B **40**, 4419 (1989).

[11]I. G. Gorlova and Yu. I. Latyshev, Pis'ma Zh. Eksp. Teor. Fiz. **51**, 197 (1990) [JETP Lett. **51**, 224 (1990)].

[12]Y. Ando, N. Motohira, K. Kitazawa, J. Takeya, and S. Akita, Phys. Rev. Lett. **67**, 2727 (1991).

[13]T. Fukami and T. Kamura, Supercond. Sci. Technol. **3**, 467 (1990).

[14]J. M. Kosterlitz and D. J. Thouless, J. Phys. C **6**, 1181 (1973).

[15]V. L. Berezinskii, Zh. Eksp. Teor. Fiz. **61**, 1144 (1971) [Sov. Phys. JETP **34**, 610 (1972)].

[16]B. I. Halperin and D. R. Nelson, J. Low Temp. Phys. **36**, 599 (1979).

[17]B. Horovitz, preceding paper, Phys. Rev. B **47**, 5947 (1993).

[18]Y. J. Uemura *et al.*, Phys. Rev. Lett. **62**, 2317 (1989).

[19]K. B. Efetov, Zh. Eksp. Teor. Fiz. **76**, 1781 (1979) [Sov. Phys. JETP **49**, 905 (1979)].

[20]B. Horovitz, Phys. Rev. Lett. **67**, 378 (1991).

[21]L. V. Mikheev and E. B. Kolomeisky, Phys. Rev. B **43**, 10431 (1991).

[22]S. E. Korshunov, Europhys. Lett. **15**, 771 (1991).

[23]S. E. Korshunov and A. I. Larkin, Phys. Rev. B **46**, 6395 (1992).

[24]A. Schmidt and T. Schneider, Z. Phys. B **87**, 265 (1992).

[25]V. L. Pokrovskii and A. L. Talanov, Zh. Eksp. Teor. Fiz. **78**, 269 (1980) [Sov. Phys. JETP **51**, 134 (1980)].

[26]H. J. Schulz, Phys. Rev. B **22**, 5274 (1980).

[27]B. Horovitz, J. Phys. C **15**, 161 (1982); **15**, 175 (1982).

[28]B. Horovitz, T. Bohr, J. M. Kosterlitz, and H. J. Schulz, Phys. Rev. B **28**, 6596 (1983).

[29]D. C. Mattis and E. H. Lieb, J. Math. Phys. **6**, 304 (1965).

[30]A. Luther and I. Peschel, Phys. Rev. B **9**, 2911 (1974).

[31]D. C. Mattis, J. Math. Phys. **15**, 609 (1974).

[32]B. I. Ivlev, N. B. Kopnin, and V. L. Pokrovsky, J. Low Temp. Phys. **80**, 187 (1990).

[33]L. Bulaevskii and J. R. Clem, Phys. Rev. B **44**, 10234 (1991).

[34]J. Sólyom, Adv. Phys. **28**, 201 (1979).

[35]L. P. Gor'kov and I. E. Dzyaloshinskii, Zh. Eksp. Teor. Fiz. **67**, 379 (1974) [Sov. Phys. JETP **40**, 198 (1975)].

[36]M. Menyhard, J. Phys. A **8**, 1982 (1975).

[37]L. Mihály and J. Sólyom, J. Low Temp. Phys. **24**, 579 (1976).

[38]S. P. Obukhov, Zh. Eksp. Teor. Fiz. **72**, 1051 (1977) [Sov. Phys. JETP **45**, 550 (1977)].

[39]P. A. Lee, T. M. Rice, and R. A. Klemm, Phys. Rev. B **15**, 2984 (1977).

[40]E. H. Rezai, J. Sak, and S. Talukdar, Phys. Rev. B **19**, 4757 (1979).

[41]E. H. Rezai, J. Sak, and J. Sólyom, Phys. Rev. B **20**, 1129 (1979).

[42]D. H. Lowndes, D. P. Norton, and J. D. Budai, Phys. Rev. Lett. **65**, 1160 (1990).

[43]M. Z. Cieplak, S. Vadlamannati, S. Guha, C. H. Nien, L. Zhang, and P. Lindenfeld (unpublished).

[44]G. Blatter, B. I. Ivlev, and J. Rhyner, Phys. Rev. Lett. **66**, 2392 (1991).